



## Balancing the Interplay Between Ligand Ejection and Therapeutic Window Light Absorption in Ruthenium Polypyridyl Complexes

Journal:	<i>Dalton Transactions</i>
Manuscript ID	DT-ART-04-2022-001237.R1
Article Type:	Paper
Date Submitted by the Author:	13-Jun-2022
Complete List of Authors:	McCullough, Annie; Tusculum University, Natural Sciences Chen, Jiaqi; Florida State University Valentine, Nathaniel; Tusculum University, Natural Sciences Franklin, Toney; Tusculum University, Natural Sciences Cantrell, Andrew; Tusculum University, Natural Sciences Darnell, Vayda; Tusculum University, Natural Sciences Qureshi, Qasim; University of Virginia College at Wise Hanson, Kenneth; Florida State University, ; Shell, Steven; University of Virginia College at Wise Ashford, Dennis; Tusculum University, Natural Sciences;

## Balancing the Interplay Between Ligand Ejection and Therapeutic Window Light Absorption in Ruthenium Polypyridyl Complexes

Annie M. McCullough<sup>†#</sup>, Jiaqi Chen<sup>§#</sup>, Nathaniel P. Valentine<sup>†</sup>, Toney M. Franklin<sup>†</sup>, Andrew P. Cantrell<sup>†</sup>, Vayda M. Darnell<sup>†</sup>, Qasim Qureshi<sup>‡</sup>, Kenneth Hanson<sup>§</sup>, Steven M. Shell<sup>‡</sup>, Dennis L. Ashford<sup>\*,†</sup>

<sup>†</sup>Department of Natural Sciences, Tusculum University, Greeneville, Tennessee 37745, United States

<sup>§</sup>Department of Chemistry & Biochemistry, Florida State University, Tallahassee, Florida 32306, United States

<sup>‡</sup>Department of Natural Sciences, University of Virginia College at Wise, Wise, Virginia, 24293, United States

<sup>#</sup>Authors contributed equally

### Abstract

Ruthenium polypyridyl complexes have gained significant interest as photochemotherapies (PCTs) where their excited-state properties play a critical role in the photo-cytotoxicity mechanism and efficacy. Herein we report a systematic electrochemical, spectrochemical, and photophysical analysis of a series of ruthenium(II) polypyridyl complexes of the type  $[\text{Ru}(\text{bpy})_2(\text{N-N})]^{2+}$  (where bpy = 2,2'-bipyridine; N-N is a bidentate polypyridyl ligand) designed to mimic PCTs. In this series, the N-N ligand was modified through increased conjugation and/or incorporation of electronegative heteroatoms to shift the metal-to-ligand transfer (MLCT) absorptions near the therapeutic window for PCTs (600 – 1100 nm) while incorporating steric bulk to trigger photoinduced ligand dissociation. The lowest energy MLCT absorptions were red-shifted from  $\lambda_{\text{max}} = 454$  nm to 564 nm, with emission energies decreasing from  $\lambda_{\text{max}} = 620$  nm to 850 nm. Photoinduced ligand ejection and temperature-dependent emission studies revealed an important interplay between red-shifting MLCT absorptions and accessing the dissociative  $^3\text{dd}^*$  states, with energy barriers between the  $^3\text{MLCT}^*$  and  $^3\text{dd}^*$  states ranging from  $850\text{ cm}^{-1}$  to  $2580\text{ cm}^{-1}$  for the complexes measured. This work demonstrates the importance of understanding both the MLCT manifold and  $^3\text{dd}^*$  state energy levels in the future design of ligands and complexes for PCT.

### Introduction

Transition metal coordination complexes have emerged as a promising class of chemotherapeutics for the treatment of cancer and other diseases.<sup>1, 2</sup> Nearly half of all chemotherapeutics administered today are derived from the platinum-based drug family (platins), which still suffer from major drawbacks, most notably harsh side-effects due to lack of specificity of malignant cells over healthy ones.<sup>3-10</sup> Photochemotherapy (PCT) and photodynamic therapy (PDT) have the potential to circumvent these issues by utilizing a compound that is minimally toxic in the dark and in its native state, but becomes cytotoxic upon illumination, providing spatiotemporal control of toxicity.<sup>11-14</sup> Traditionally, PDTs rely on the photoinduced excited-state electron transfer (Type I) or excited-state triplet energy transfer (Type II) to molecular oxygen ( $^3\text{O}_2$ ) to generate reactive oxygen species (ROS) and trigger

oxidative cell death.<sup>11</sup> While PDTs have been used in clinical oncology for over 40 years, they have largely remained absent from main-stream cancer treatments due to two major factors; 1) the inherent hypoxic nature of tumor cells and 2) a lack of PSs that absorb light in the near-IR, therapeutic window (600 - 1100 nm).<sup>15-22</sup> In contrast, PCTs mechanism of toxicity involves the photoinduced release of a therapeutic reagent, making it oxygen-independent and circumventing the issue of low cellular oxygen concentrations.<sup>21, 23-29</sup> Ru(II) polypyridyl compounds have shown great promise as PCTs due to their synthetic viability, relatively long-lived triplet metal-to-ligand charge transfer (<sup>3</sup>MLCT\*) excited states, and well understood photophysical behavior.<sup>30-36</sup>

Ru(II) PCTs typically undergo photoinduced ligand loss to either release a known cytotoxic organic compound from the coordination sphere<sup>24, 37-41</sup> or generate a di-solvated activated metal species that can have cisplatin-like interactions with DNA at the newly opened coordination sites (Figure 1).<sup>23, 29, 42-44</sup> While this mechanism has been shown to have high phototoxicity indexes, most reported Ru(II) PCTs only absorb in the blue region of the electromagnetic spectrum (<485 nm), which penetrates skin much shallower than longer wavelengths.<sup>22</sup> Near-IR ligand ejection has been reported for Ru(II) PCTs, however these complexes still have relatively low oscillator strengths at wavelengths >500 nm and center around the ejection of a monodentate ligand as opposed to bidentate ligand ejection required for metalation of DNA.<sup>21, 25, 37, 42, 45, 46</sup>

Photoinduced ligand ejection from the octahedral Ru(II) center requires thermal population of the formally anti-bonding <sup>3</sup>dd\* states from the <sup>3</sup>MLCT\* excited-states.<sup>30, 47-49</sup> This is typically achieved by increasing steric bulk around the Ru(II) center, distorting the pseudo-octahedral, and ultimately lowering the energy the <sup>3</sup>dd\* states. In addition, incorporation of increased conjugation and/or electronegative heteroatoms within the ligand framework lowers the energies of the ligand  $\pi^*$  orbitals, increasing their  $\pi^*$ -acceptor ability, and resulting in lower MLCT energy absorption features.<sup>30, 50-52</sup> Furthermore, the compound must be soluble in biological (aqueous) medium and one must strike a balance between thermal stability of the native complex and photoactivation kinetics. Papish and co-workers recently published DFT analyses of a series of Ru(II) polypyridyl complexes bearing acidic protons and note the importance of understanding these excited-state energy levels in PCT design and the pronounced effect they can have on the photo-toxicity mechanism.<sup>53</sup>

With this in mind, we set out to design a series of compounds with the general structure [Ru(bpy)<sub>2</sub>(N-N)]<sup>2+</sup> (where N-N is a bidentate polypyridyl ligand, Figure 1) that systematically increases steric bulk around the Ru(II) center while also introducing increased conjugation and/or electronegative heteroatoms. The goal being to understand their electrochemical, spectrochemical, ligand ejection kinetics, photophysical properties, and ability to act as PCTs. This work demonstrates that traditional ligand design strategies to red-shift MLCT absorptions by lowering the energy of the ligand  $\pi^*$  orbitals can also impact ligand dissociation kinetics by limiting the accessibility of the <sup>3</sup>dd\* states, and ultimately the ability of a complex to act as a PCT agent. The present study further highlights the importance of understanding this

relationship between ligand ejection kinetics and lower energy absorption in Ru(II) PCTs, which will aid in the design strategies of future PCT ligands and complexes.

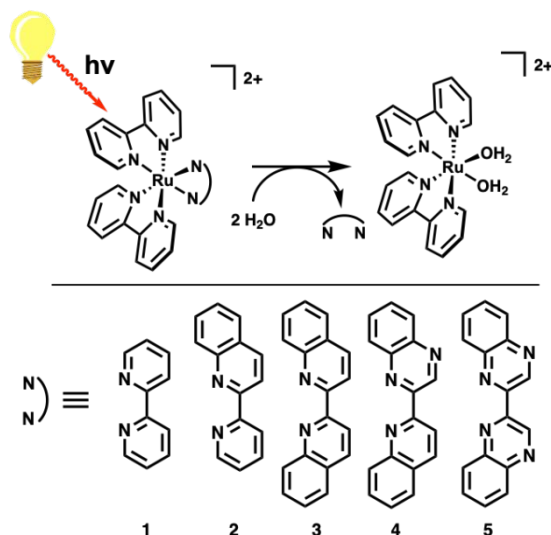
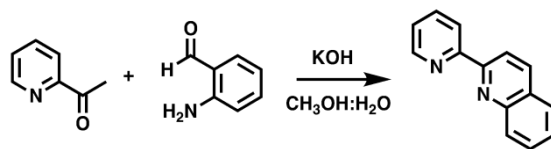


Figure 1. Photoinduced ligand ejection from Ru(II) center and structures of  $[\text{Ru}(\text{bpy})_2(\text{N-N})]^{2+}$  complexes **1-5**.

## Results and discussion:

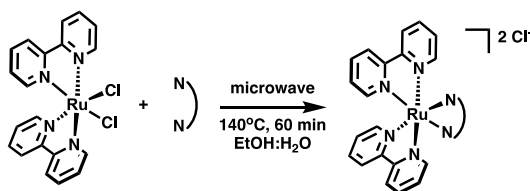
**Ligand Synthesis.** 2,2'-bipyridine (**L1**) and 2,2'-biquinoline (**L3**) were purchased and used without further purification. 2-(quinolin-2-yl)quinoxaline (**L4**) was synthesized by a reported procedure in 85% yield.<sup>30</sup> 2-(pyridin-2-yl)quinoline (**L2**) was synthesized in 96% yield using a Friedländer condensation of 2-acetylpyridine and 2-aminobenzaldehyde in the presence of a base catalyst (Scheme 1). 2,2'-biquinoxaline (**L5**) was prepared in 10% yield using minor modifications of literature procedure<sup>54</sup> (i.e., homocoupling of the hydrochloride salt of quinoxaline), with the experimental details provided in the Supporting Information.

Scheme 1. Synthesis of **L2**.



**Complex Synthesis.** The  $[\text{Ru}(\text{bpy})_2(\text{N-N})]^{2+}$  complexes were prepared as their chloride salts by the reaction of  $\text{Ru}(\text{bpy})_2\text{Cl}_2$ <sup>55</sup> with 1 equivalent of the corresponding N-N ligand in 1:1 EtOH:H<sub>2</sub>O in a microwave oven reactor at 140°C for 1 hour (Scheme 2). The reaction progress was monitored using UV-vis spectroscopy for the disappearance of the  $\text{Ru}(\text{bpy})_2\text{Cl}_2$  absorption features ( $\lambda_{\text{max}} = 363$  and 526 nm in CH<sub>3</sub>CN)<sup>56</sup> and the appearance of the absorption peaks attributed to complexes **1 – 5**. The crude mixtures were then purified by size exclusion chromatography (Sorbadox S-25 fine) to yield pure complexes. It should be noted that all of the complexes are readily soluble in aqueous media, which is important for biological applications.

Scheme 2. General procedure for the synthesis of complexes **1-5**.



**Electrochemistry.** The electrochemical properties of complexes **1** – **5** were analyzed in dry CH<sub>3</sub>CN (0.1 M TBAPF<sub>6</sub> supporting electrolyte, where TBAPF<sub>6</sub> = tetrabutyl ammonium hexafluorophosphate) by cyclic and square-wave voltammetry. The  $E_{1/2}$  for the Ru<sup>3+/2+</sup> redox couple (Equation 1) for each complex are reported in Table 1 with cyclic voltammograms shown in Figure 2.

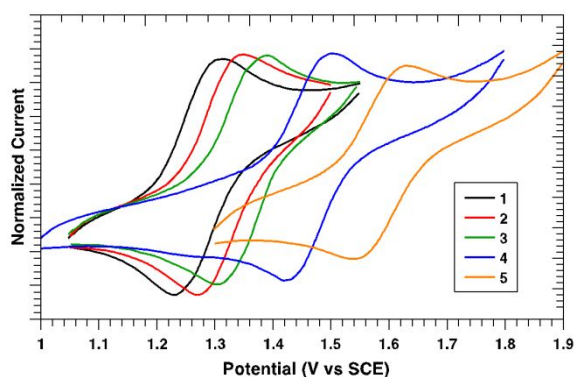
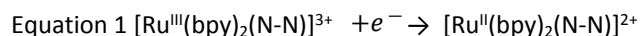


Figure 2. Cyclic voltammograms acquired at 100 mV/s for 1 mM solutions of **1-5** in N<sub>2</sub> deaerated CH<sub>3</sub>CN with 0.1 M TBAPF<sub>6</sub> supporting electrolyte. GC working electrode, graphite rod counter electrode, and Ag/AgNO<sub>3</sub> reference electrode (0.01 M AgNO<sub>3</sub> with 0.1 M TBAPF<sub>6</sub> in CH<sub>3</sub>CN). Values were adjusted to agree with literature values for [Ru(bpy)<sub>3</sub>]<sup>3+/2+</sup> at 1.29 V vs SCE.<sup>57</sup>

Table 1. Electrochemical properties of **1-5** in N<sub>2</sub> deaerated CH<sub>3</sub>CN (0.1 M TBAPF<sub>6</sub> electrolyte).

Compound	$E_{1/2}(\text{Ru}^{3+/2+})$	$E_{1/2}(\text{Ru}^{2+/+})$	$E_{1/2}(\text{Ru}^{+/0})$	$E_{1/2}(\text{Ru}^{0/1-})$
1	1.29	-1.35	-1.55	-1.78
2	1.32	-1.12	-1.50	-1.74
3	1.37	-0.92	-1.38	-1.69
4	1.48	-0.64	-1.24	-1.62
5	1.60	-0.46	-1.08	-1.61

In CH<sub>3</sub>CN deaerated with Ar for 10 min, 1 mM in complex and 0.1 M TBAPF<sub>6</sub> supporting electrolyte. GC working electrode, graphite rod counter electrode, and Ag/AgNO<sub>3</sub> (0.01 M AgNO<sub>3</sub> with 0.1 M TBAPF<sub>6</sub> in CH<sub>3</sub>CN) reference (values were adjusted to agree with literature values for [Ru(bpy)<sub>3</sub>]<sup>3+/2+</sup> at 1.29 V vs SCE).<sup>34, 51, 56, 57</sup>  $E_{1/2}$  values from differential pulse voltammetry.

All complexes exhibit reversible Ru<sup>3+/2+</sup> redox couples with  $E_{1/2}$  values ranging from 1.29 V for **1** to 1.60 V for **5** (vs SCE). Complexes **2** - **5** exhibit a more positive Ru<sup>3+/2+</sup> couple compared to the parent [Ru(bpy)<sub>3</sub>]<sup>2+</sup> (**1**). This shift due to changes in N-N can be rationalized by the increased

conjugation and/or the addition of electronegative heteroatoms compared to bpy, decreasing the energy of  $\pi^*$  orbitals of N-N. This results in increased  $d\pi - \pi^*$  back bonding from the  $Ru^{II}$  center to the N-N ligand, stabilizing the  $d\pi^6$  electronic configuration, and ultimately increasing the redox potential for the  $Ru^{3+/2+}$  couple.<sup>30, 58-60</sup>

Each complex exhibits three reversible ligand-based reductions with representative CVs shown in Figure 3 (all shown in Figure S1) and potentials listed in Table 1. The first ligand-based reduction ( $Ru^{2+/+}$ , Equation 2) for **2** - **5** are at more positive potentials compared to **1** (-1.35 V vs SCE), ranging from -1.12 V for **2** to -0.46 V (vs SCE) for **5**. The significantly more positive reduction potential for **4** (-0.64 V vs SCE) and **5** (-0.46 V vs SCE) are noteworthy given the possibility for these complexes to be reduced intracellularly by biological reducing agents such as NADH ( $\approx -0.56$  V vs SCE in  $H_2O$ <sup>61</sup>) or GSH ( $\approx -0.48$  V vs SCE in  $H_2O$ <sup>62</sup>). Again, the increased conjugation and incorporation of heteroatoms stabilizes the  $\pi^*$  acceptor levels of N-N, resulting in lower reduction potentials of the N-N ligand.

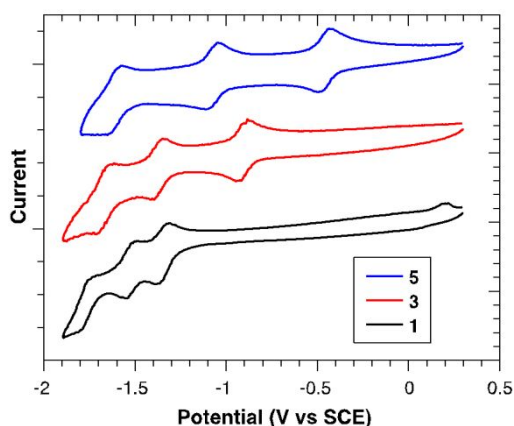
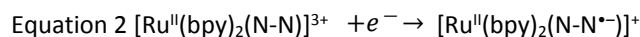
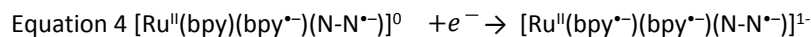
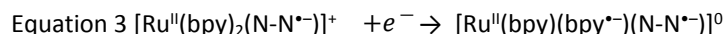


Figure 3. Cyclic voltammograms acquired at 100 mV/s for 1 mM solutions of **1** (black), **3** (red), and **5** (blue) in Ar deaerated  $CH_3CN$  with 0.1 M  $TBAPF_6$  supporting electrolyte. GC working electrode, graphite rod counter electrode, and  $Ag/AgNO_3$  reference electrode (0.01 M  $AgNO_3$  with 0.1 M  $TBAPF_6$  in  $CH_3CN$ ). Values were adjusted to agree with literature values for  $[Ru(bpy)_3]^{3+/2+}$  at 1.29 V vs SCE.<sup>57</sup>

The variation in the first reduction potentials ( $Ru^{2+/+}$ , 0.89 V) is significantly larger than the variance for the second reduction ( $Ru^{+/0}$ , 0.47 V) and third reduction ( $Ru^{0/1-}$ , 0.17 V) potentials for the series (see Table 1 and Figure S2). This demonstrates, as expected, that the first reduction of the complex is largely N-N ligand-centered (Equation 2), with the second and third reductions occurring mainly on the remaining bpy ligands (Equation 3 & Equation 4).



**UV-Vis Absorption.** UV-Vis absorption spectra of complexes **1** – **5** in water (Figure 4) all feature intense  $\pi \rightarrow \pi^*$  absorption features below 350 nm ( $\epsilon \approx 4.0 \times 10^4 - 7.0 \times 10^4 \text{ M}^{-1} \text{ cm}^{-1}$ ). Complexes **3** – **5** exhibit additional, lower energy and structured absorption transitions at 350 – 450 nm that are attributed to the  $\pi \rightarrow \pi^*$  transition of the N-N ligands.<sup>30</sup> The complexes also exhibit broad, lower-energy metal-to-ligand charge-transfer (MLCT) transitions ranging from 400 nm to 600 nm ( $\epsilon \approx 0.56 \times 10^4 - 11.6 \times 10^4 \text{ M}^{-1} \text{ cm}^{-1}$ ) and are formally assigned as a  $[d\pi^6] \rightarrow [d\pi^5\pi_1^*]^1$  transitions.<sup>49, 52, 63</sup> The appearance of the nominally spin forbidden  $[d\pi^6] \rightarrow [d\pi^5\pi_1^*]^3$  transition at longer wavelengths (>600 nm) is due to spin-orbit coupling, but still have low oscillator strengths and therefore low molar absorptivities.<sup>49, 52, 63</sup> As mentioned previously, shifting the absorptions to lower energies is desirable to move excitation and photo-induced ligand ejection towards the therapeutic window of PCTs (>600 nm). This trend is observed in Figure 4 by the red shift in the series from <sup>1</sup>MLCT  $\lambda_{max} = 454 \text{ nm}$  (**1**) to  $\lambda_{max} = 564 \text{ nm}$  (**5**).

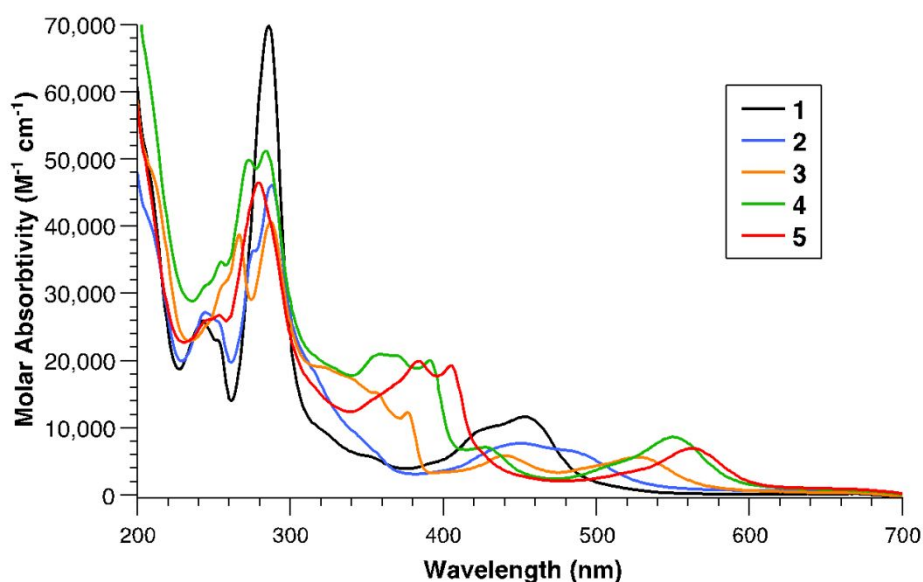


Figure 4. UV-vis absorption spectra of complexes **1** – **5** in H<sub>2</sub>O.

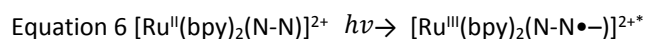
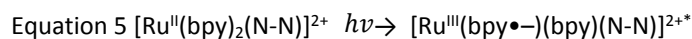
Table 2. Spectroscopic and ligand ejection properties for the complexes **1** – **5**

Compound	Absorbance $\lambda$ (nm) ( $\epsilon, \times 10^3 \text{ M}^{-1} \text{ cm}^{-1}$ ) <sup>a</sup>	$K_{pld} (\text{s}^{-1})$ <sup>b</sup>	Emission at rt <sup>c</sup>			$k_r (\times 10^4 \text{ s}^{-1})$ <sup>d</sup>	$k_{nr} (\times 10^6 \text{ s}^{-1})$ <sup>e</sup>
			$\lambda_{max}$ (nm)	$\tau$ (ns)	$\Phi_{PL}$		

<b>1</b>	454 (11.6)	-	620	550	0.042	7.6	1.7
	417 (8.7)						
	286 (69.9)						
<b>2</b>	489 (6.2)	$4.3 \times 10^{-5}$	710	195	0.006	2.9	4.9
	450 (7.6)						
	288 (46.2)						
<b>3</b>	527 (5.6)	$2.3 \times 10^{-4}$	760	125	0.006	4.8	8.0
	440 (5.8)						
	287 (40.6)						
<b>4</b>	551 (8.6)	-	830 <sup>f</sup>	13	-	-	-
	426 (7.1)						
	285 (51.2)						
<b>5</b>	564 (6.9)	-	850 <sup>f</sup>	22	-	-	-
	404 (19.2)						
	279 (46.3)						

<sup>a</sup>Measured in H<sub>2</sub>O. <sup>b</sup>Measured in H<sub>2</sub>O utilizing the light from a Kessil PR160 (467 nm, 120 mW/cm<sup>2</sup> at 5 cm) illuminated a quartz cuvette containing 3 mL of solutions of known concentration 5 cm away from the light source. Light intensity was adjusted to correct for varying molar absorptivities. <sup>c</sup>Emission data acquired using dilute solutions and lifetimes calculated from monoexponential fits. <sup>d</sup> $k_r = \phi/\tau$ . <sup>e</sup> $k_{nr} = (1-\phi)/\tau$ . <sup>f</sup>Emission maxima from reference<sup>30</sup> as acquired in MeCN.

The energies of the MLCT transition are influenced by both an increase in conjugation within the N-N ligand, and the incorporation of non-coordinating electronegative heteroatoms. These perturbations lower the energies of the  $\pi^*$  orbitals on the N-N ligand, increasing the  $\pi^*$  - acceptor ability of the ligand, resulting in lower MLCT energy absorption features.<sup>30, 50-52</sup> Complexes **3**, **4**, and **5** exhibit splitting of the MLCT manifolds that arise from charge transfer from the Ru<sup>II</sup> center to the bpy (Equation 5) and N-N (Equation 6)  $\pi^*$ -orbitals for the higher and lower energy transitions, respectively.<sup>30</sup> The energy difference between the MLCT transitions increases as the  $\pi^*$  acceptor ability of the N-N ligand increases.



**Photoinduced Ligand Ejection.** PCT photo-toxicity mechanism requires the loss of a ligand under illumination, in particular, a bidentate ligand for DNA metalation.<sup>23, 44, 64, 65</sup> The rate constant for ligand dissociation ( $k_{pld}$ ) for each complex was monitored using the apparatus shown in Figure S3 with UV-vis spectra acquired at known time intervals during illumination with 467 nm light. The intensity of the light source was adjusted in accord with the molecule's molar absorptivities to generate an approximately equal number of excited states during photolysis (see Table S1). Representative UV-vis spectra of complexes **3** and **4** under illumination are shown in Figure 5 with all of the spectra shown in the Supporting Information (Figure S4).



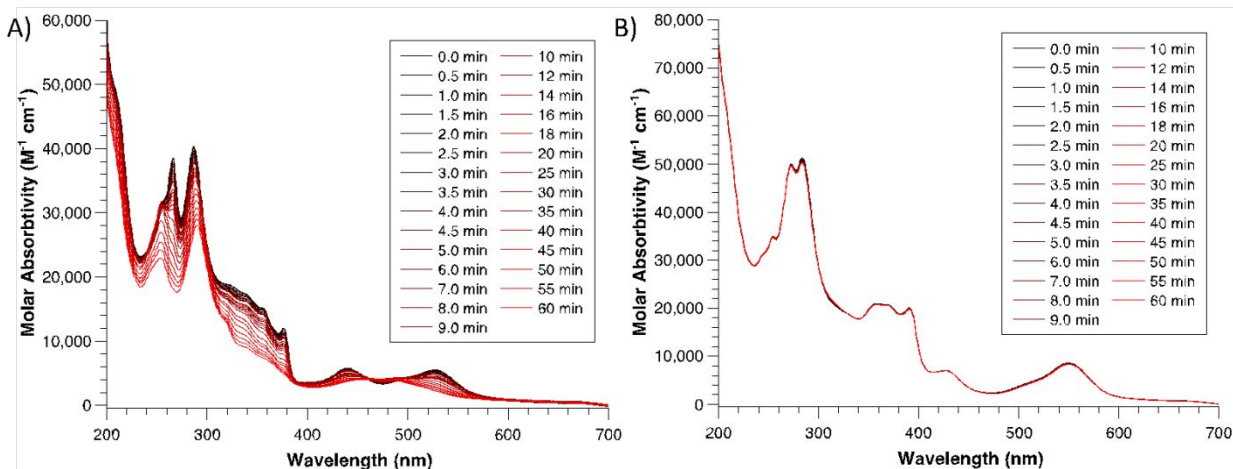
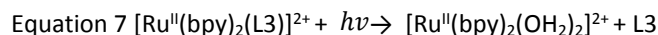


Figure 5. Absorption spectra of complexes **3** (A) and **4** (B) in 3 mL H<sub>2</sub>O monitored over time during irradiation with light from a Kessil PR160 (467 nm, 120 mW/cm<sup>2</sup> at 5 cm). Light intensity was adjusted to correct for varying molar absorptivities at 467 nm (75% for **3** and 100% for **4**).

As can be seen in Figure 5 and Figure S4, only complex **3** undergoes a dramatic spectral change over the one hour of irradiation, including a decrease in intensity of the MLCT transition at 530 nm as well as the  $\pi \rightarrow \pi^*$  transition from 320–380 nm. The resulting spectrum is in good agreement with the spectrum previously reported for [Ru(bpy)<sub>2</sub>(OH<sub>2</sub>)<sub>2</sub>]<sup>2+</sup>.<sup>23, 66, 67</sup> Observations are consistent with the photoinduced ejection of the N–N ligand upon irradiation of **3** (Equation 7).<sup>23, 68, 69</sup> All of the complexes were stable in solution in the dark for over a year (Figure S5).



Of the remaining complexes, only **2** exhibits spectral changes under 467 nm illumination while **1**, **4**, and **5** are largely unperturbed (Figure S4). The kinetics for the photoinduced ligand ejection for **2** and **3** were fit to a first order reaction equation (Figure 6) with the rate constants ( $k_{\text{pld}}$ ) being reported in Table 2. As expected, the increase in steric bulk resulted in increased  $k_{\text{pld}}$  in the order **1** ( $< < 10^{-6} \text{ s}^{-1}$ )  $< \textbf{2}$  ( $4.3 \times 10^{-5} \text{ s}^{-1}$ )  $< \textbf{3}$  ( $2.3 \times 10^{-4} \text{ s}^{-1}$ ). In contrast and unexpectedly, despite increased steric bulk around the Ru(II) center for **4** and **5**, which results in lowering the energy of the formally anti-bonding <sup>3</sup>dd\* states that lead to ligand dissociation,<sup>47, 70, 71</sup> complexes **4** and **5** remained largely intact. To ensure lack of photoreactivity was not due to differences in molar absorptions the same experiments were conducted with a broad spectrum white-LED lamp, which showed the same general trends and relative differences in  $k_{\text{pld}}$  as described above (see Figure S5).

As first reported by Glazer and co-workers, and confirmed under the same conditions used here, [Ru(bpy)<sub>2</sub>(6,6'-dmb)]<sup>2+</sup> (where 6,6'-dmb = 6,6'-dimethyl-2,2'-bipyridine) undergoes complete ligand dissociation in under a minute of illumination (see Figure S6).<sup>23</sup> However, it should be noted that while the increased steric bulk in **3**, **4**, and **5** distorts the pseudo-octahedral around the Ru(II) center lowering the <sup>3</sup>dd\* states, the introduction of non-coordinating electronegative heteroatoms in **4** and **5** also lower the N–N  $\pi^*$  orbitals and the

energy of the  $^3\text{MLCT}$  states.<sup>30, 47</sup> This may result in the ligand dissociative  $^3\text{dd}^*$  states being inaccessible at room temperature, as will be discussed in the next section.

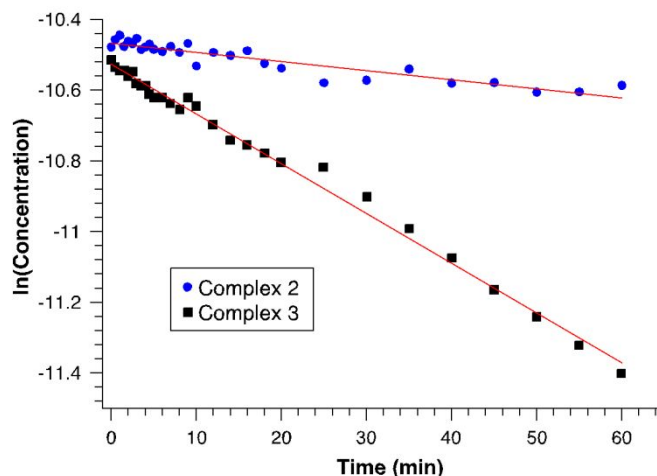


Figure 6. First order fits (red lines) for photoinduced ligand dissociation of  $\ln(\text{concentration})$  versus time for complexes **2** (blue) and **3** (black).

### Emission Spectroscopy

The steady-state and time-resolved emission for the complexes in  $\text{H}_2\text{O}$  were acquired under 445 nm excitation and the results are shown in Figure 7 and summarized in Table 2. The maximum emission energy decreases in the order **1** (620 nm) > **2** (710 nm) > **3** (760 nm). Due to instrument limitations (i.e., low signal beyond 800 nm), we were unable to determine emission maxima for **4** and **5** in  $\text{H}_2\text{O}$  (see Figure S7 & S8). However, the emission onset was similar to that previously reported for **4** and **5** in MeCN (830 and 850 nm, respectively),<sup>30</sup> consequently those values were included in Table 2 and used for further analysis.

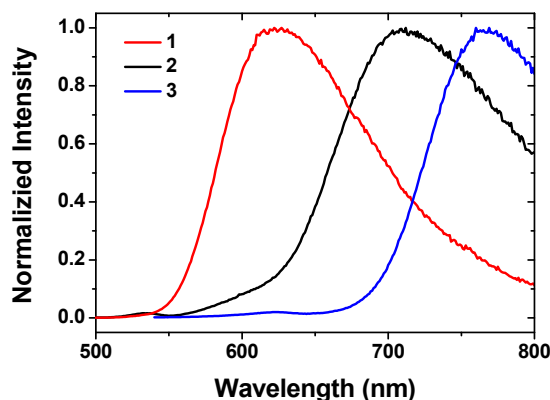


Figure 7. Normalized emission spectra of **1**, **2** and **3** in  $\text{N}_2$  deaerated  $\text{H}_2\text{O}$  ( $\lambda_{\text{ex}} = 445 \text{ nm}$ ).

Previous analyses has shown a linear relationship between the electrochemical gap  $\Delta E_{1/2}$ , (i.e.,  $\Delta E_{1/2} = E_{1/2}(\text{Ru}^{3+/2+}) - E_{1/2}(\text{Ru}^{2+/+})$ ) and the absorption/emission maxima of ruthenium(II) polypyridyl complexes.<sup>48, 57, 72, 73</sup> Figure 8 presents how the lowest energy absorption ( $\bar{\nu}_{\text{abs}}$ ) and

emission ( $\bar{\nu}_{em}$ ) maxima vary with  $\Delta E_{1/2}$ . Both absorption and emission energies exhibit a linear relationship with  $\Delta E_{1/2}$ , expected for transitions to and from MLCT excited states.<sup>48, 72, 74</sup>

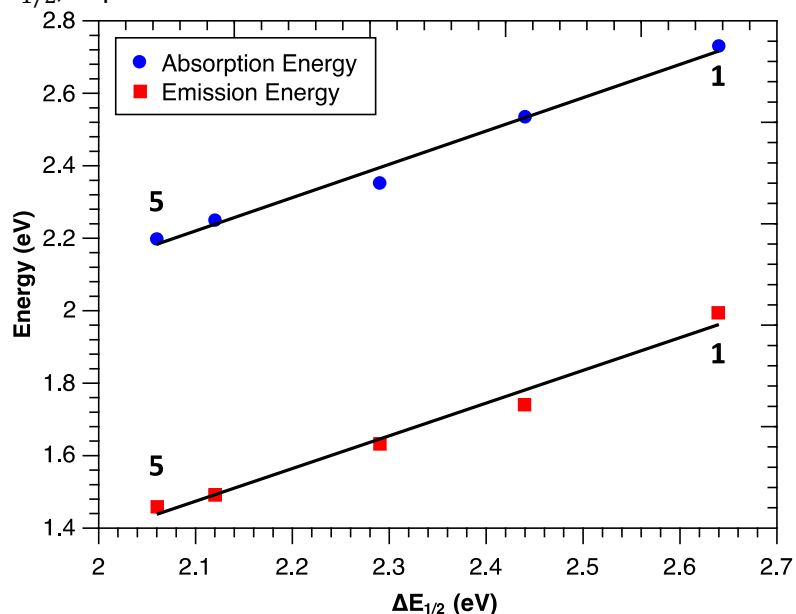


Figure 8. Variation of absorption (blue circle), and emission (red squares) maximum energies with the electrochemical gap ( $\Delta E_{1/2} = E_{1/2}(Ru^{3+/2+}) - E_{1/2}(Ru^{2+/+})$ ) for complexes **1** – **5** (right-to-left) in  $H_2O$ . Note that emission energies for complexes **4** and **5** are from reported values.<sup>30</sup>

Time-resolved emission kinetics were monitored at the emission peak maxima for **1** - **3** and at 800 nm for **4** - **5**. The emission decays were fit with a singlet exponential function and the results are summarized in Table 2. The emission lifetime decreases in the order **1** (550 ns) > **2** (195 ns) > **3** (125 ns) > **4** (13 ns)  $\approx$  **5** (22 ns). The approximately linear relationship between the excited state lifetime and maximum emission energy is in good agreement with that expected by the energy gap law (Figure 9).<sup>75</sup>

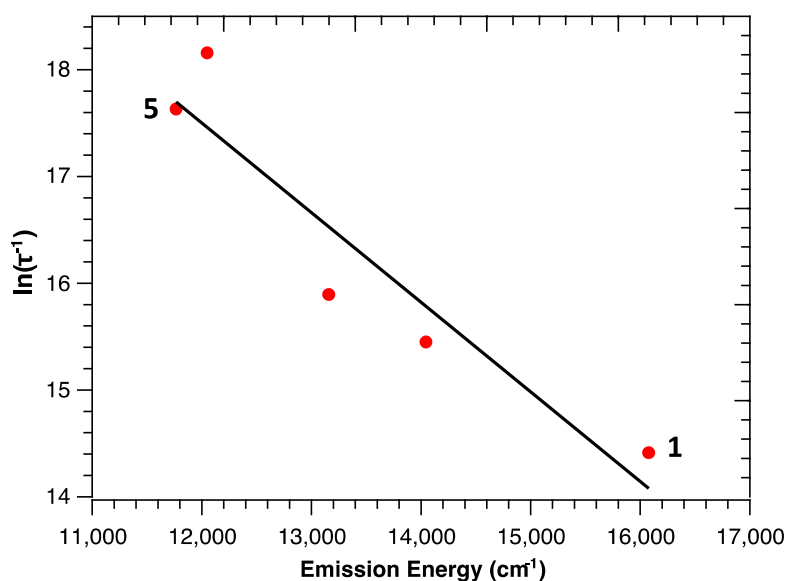


Figure 9. Plot of emission energy vs  $\ln \tau^{-1}$  for complexes **1** – **5** (right-to-left) in H<sub>2</sub>O at 25°C.

### Temperature Dependent Emission

As noted above, ligand dissociation for ruthenium(II) polypyridyl complexes is typically attributed to thermal population of the formally antibonding metal-centered <sup>3</sup>dd\* state from the <sup>3</sup>MLCT\* manifold.<sup>71, 75</sup> Temperature-dependent emission lifetime measurements is a strategy that can be used to determine the activation energy barrier ( $\Delta E_{pld}$ , energy gap for photoinduced ligand dissociation) between the <sup>3</sup>MLCT\* and <sup>3</sup>dd\* states.<sup>52</sup> Here we monitored changes in the excited state lifetime of **1** - **3** with respect to temperature with example decay curves show in Figure 10 for **1** and temperature dependent lifetimes summarized in Figure 11 (all emission decays are shown in Figures S9 – S11).

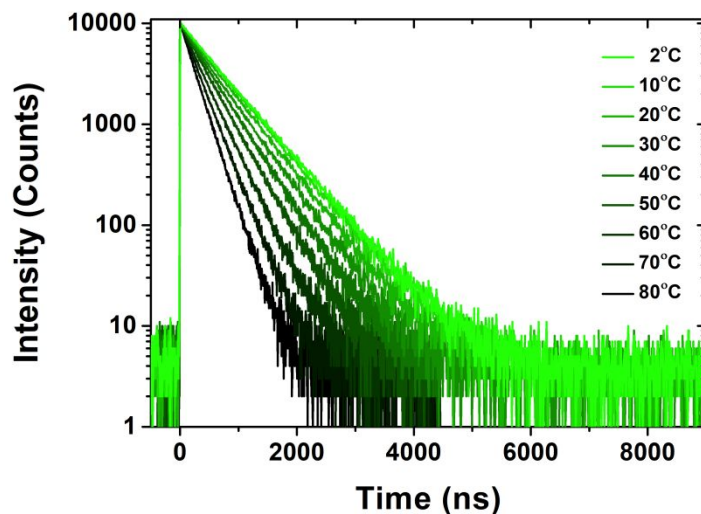


Figure 10. Emission decays for **1** in N<sub>2</sub> deaerated H<sub>2</sub>O at various temperatures ( $\lambda_{ex} = 405$  nm,  $\lambda_{em} =$  emission maximum).

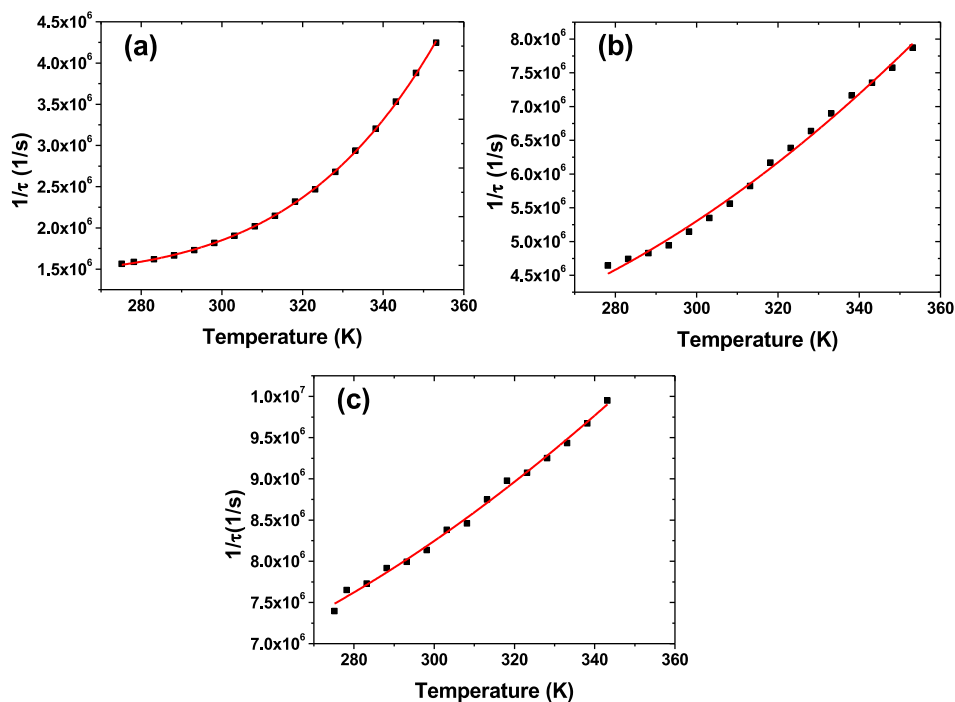


Figure 11. Plot of  $1/\tau$  versus temperature for complexes **1** (a), **2** (b) and **3** (c) in  $N_2$  deaerated  $H_2O$ .

As expected, the excited state lifetime of all complexes decreases with increasing temperature. The results were then fit with Equation 8 where  $\tau(T)$  is the lifetime at a given temperature ( $T$ ),  $R$  is the ideal gas constant,  $k^0$  is a pre-exponential factor, and  $k$  is the sum of radiative and non-radiative decay rates ( $k = k_r + k_{nr}$ ).<sup>52</sup> The results of the fitting are summarized in Table 3.

$$\text{Equation 8 } \frac{1}{\tau(T)} = k + k^0 \exp \left[ -(\Delta E_{pld} / RT) \right]$$

Table 3. Fitting parameters for the temperature dependent emission kinetics for **1-3** in  $N_2$  deaerated  $H_2O$ .

Sample	$k$ ( $\times 10^6 \text{ s}^{-1}$ )	$k^0$	$\Delta E_{pld}$ ( $\text{cm}^{-1}$ )
<b>1</b>	1.4	$1.1 \times 10^{11}$	2580
<b>2</b>	2.8	$3.0 \times 10^8$	1000
<b>3</b>	5.8	$1.5 \times 10^8$	850

The energy gap,  $\Delta E_{pld}$ , of  $[Ru(bpy)_3]^{2+}$  (**1**) of  $2580 \text{ cm}^{-1}$  is in reasonable agreement with those previously obtained for **1** in aqueous conditions, where  $\Delta E_{pld}$  is attributed to the thermal barrier to excited state deactivation via metal centered  $^3dd^*$  states.<sup>76</sup> The  $\Delta E_{pld}$  for the complexes measured here decreases in the order **1** ( $2580 \text{ cm}^{-1}$ ) > **2** ( $1000 \text{ cm}^{-1}$ ) > **3** ( $850 \text{ cm}^{-1}$ ), which correlates with the trend of decreasing lifetime. This trend in  $\Delta E_{pld}$  also inversely correlates with the increasing rate constant for photoinduced ligand ejection,  $k_{pld}$ , in the order **3** > **2** >> **1**, further reinforcing the hypothesis that population of the  $^3dd^*$  states is responsible for ligand dissociation. It should also be noted that ligand dissociation from the  $^3dd^*$  state is rapid

compared to relaxation back to the MLCT manifold and/or ground state.<sup>48, 52, 77</sup> Consequently, the more than 1000 cm<sup>-1</sup> greater  $\Delta E_{pld}$  is responsible for the increased stability and lack of ligand dissociation for **1**, as compared to **2** and **3**. Unfortunately, due to their short lifetimes and our limited detector response, attempts to measure temperature dependent lifetimes for **4** and **5** under the same conditions were unsuccessful. The importance in the observed variation of  $\Delta E_{pld}$  energies and PCT design will be discussed below.

### Cytotoxicity Assays

MTT (3-[4,5-dimethylthiazol-2-yl]-2,5 diphenyl tetrazolium bromide) dye reduction assays were used to analyze the potential biological activity of complexes **1** – **5** against human embryonic kidney (HEK293T) cells cultures (Figure S12) with and without illumination. Briefly, HEK293T cells were seeded into 96-well plate and dosed with varying concentrations of the complexes. The cultures were then either exposed to 467 nm illumination for 60 minutes, or covered from irradiation *in situ* (see SI for full experimental details). Overall, as might be expected from the outcomes above, the complexes displayed relatively low cytotoxicity with or without illumination. However, all of the complexes except for **2** displayed statistically significant increased cytotoxicity under illumination compared to non-irradiated samples at the 200  $\mu$ M concentration (Figure S12). Control experiments with HEK293T cells, with and without illumination, showed no light dependence with cisplatin and a significant dependence with  $[\text{Ru}(\text{bpy})_2(6,6'\text{-dmb})]^{2+}$ , as expected (see Figure S14).

Due to concerns of overheating the samples and causing cell death, all cytotoxicity studies under illumination were carried out at 25% of the 467 nm lamp intensity. As a result, to correct for variations in absorptivity of the complexes at 467 nm, the difference in cell viability between illuminated and non-illuminated samples were divided by their molar absorptivities (Table S1) to give a comparison between the complexes (Figure S13). As expected, **3** had the highest photoinduced cytotoxic behavior, however unexpectedly, **5** showed the second highest when correcting for these absorptivity differences. While these results demonstrate the ability of the complexes to act as phototoxic agents, further studies are needed to better understand their cytotoxic behavior, in addition to designing new and more active compounds based upon the discussion given below.

### Balancing Absorption in Therapeutic Window and Ligand Ejection

As has been previously discussed, current PCTs suffer from minimal absorption within the 'therapeutic window' to be candidates for clinical oncology use. Given the understanding of Ru(II) polypyridyl light absorption and photophysics, we set out to design a new series of PCTs that incorporated increased conjugation and/or electronegative heteroatoms to shift the absorption closer to the therapeutic window. At the same time, the series also introduced steric bulk around the metal center to promote photoinduced ligand ejection, a key step in the cytotoxicity mechanism. However, as demonstrated here and poignantly exemplified with complexes **3** and **4**, one must strike a balance between shifting absorptions to longer wavelengths and the accessibility of the dissociative <sup>3</sup>dd\* excited states. As shown in Figure 5, **3** undergoes ligand loss under 467 nm illumination with a first order rate constant of  $2.3 \times 10^{-4} \text{ s}^{-1}$  where **4** shows no measurable dissociation. Sterically, there is little to no difference in the

ligands, suggesting that the dissociative  $^3dd^*$  state is at the same relative energy in both. However, the introduction of a single electronegative heteroatom to the periphery of **4** resulted in a lowering of  $^1MLCT$  excitation by 0.10 eV (527 nm for **3** and 551 nm for **4**) and  $^3MLCT$  emission by 0.14 eV (760 nm for **3** and 830 nm for **4**). As a result of lowering the  $MLCT^*$  states,  $\Delta E_{pld}$  increases for **4** compared to **3** (see Figure 12). This makes the dissociative  $^3dd^*$  states inaccessible at room temperature for **4**, ultimately inhibiting photoinduced ligand ejection.

These findings demonstrate that in the pursuit of complexes designed to act as PCTs one must closely consider the excited-state manifolds and effect shifting energies can have on the compounds ability to act as a phototoxic agent. In the series of compounds reported herein, the introduction of a single electronegative heteroatom shut off the cytotoxicity of the complex, despite significant strain around the metal center. These understandings will aid in the future design of PCTs to help strike a balance between therapeutic window absorption, thermal stability, and photoactivation kinetics that is critical for successful clinical adoption of PCTs.

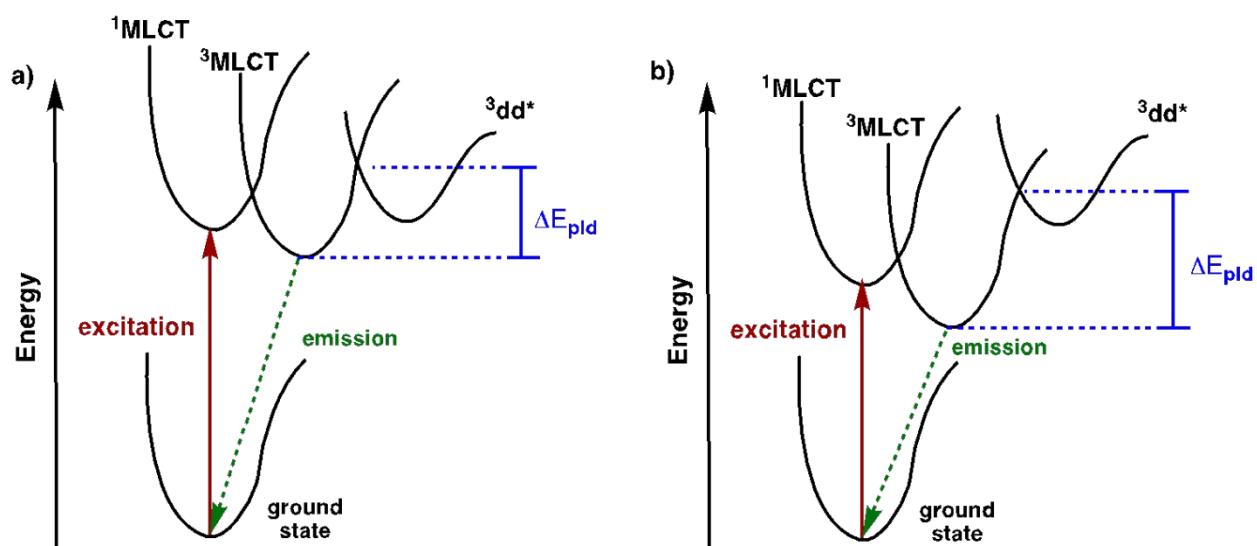


Figure 12. Excited state diagrams of ruthenium polypyridyl compounds for complexes that absorb at shorter wavelengths (a, such as **3**) compared to longer wavelengths (b, such as **4**).

## Conclusions

We have described here the synthesis, characterization, spectrochemical, and photophysical analysis of a series of ruthenium(II) polypyridyl complexes of the type  $[Ru(bpy)_2(N-N)]^{2+}$  designed to be used as PCTs. The N-N bidentate ligands were selected as to introduce increased conjugation and/or electronegative heteroatom to lower the  $\pi^*$ -acceptor levels. Through the series, the lowest energy  $MLCT$  absorption maximum was red-shifted from **1** ( $\lambda_{max} = 454$  nm) to **5** ( $\lambda_{max} = 564$  nm). However, despite increased steric bulk, photolysis experiments only showed appreciable photoinduced ligand dissociation for complexes **2** ( $k_{pld} = 4.3 \times 10^{-5}$ ) and **3** ( $k_{pld} = 2.3 \times 10^{-4}$ ). Time-resolved and temperature-dependent emission studies revealed that lowering  $\pi^*$ -acceptor energy levels in the N-N ligands decreased emission energies ( $\lambda_{max} = 620$  nm for **1** to  $\lambda_{max} = 850$  nm for **5**) and increased the energy barrier ( $\Delta E_{pld}$ , 2580  $cm^{-1}$  for **1** and 850  $cm^{-1}$  for **3**) to access the dissociated  $^3dd^*$  states. This demonstrates a balancing act

between red-shifting the MLCT absorption into the 'therapeutic window' while still maintaining photoinduced ligand ejection at room temperature which can be applied to future PCT design.

### Author Contributions

AMM, NPV, TMF, APC, VMD, and DLA performed the synthesis, full characterization, and photostability studies of the reported complexes. JC performed the photophysical analysis of the complexes and QQ and SMS performed the cytotoxicity analyses. AMM, KH, and DLA did majority of the writing-original draft work with JC and SMS writing the emission and cytotoxicity sections, respectively. Brittany Gentry and Michaela Hall also assisted in the cytotoxicity studies. DLA performed the conceptualization and writing-review & editing work.

### Conflicts of Interest

There are no conflicts to declare.

### Acknowledgments

This work was supported by the Arthur Vining David Foundations, East Tennessee Foundation, and Eastman Chemical Company supporting A.M.M, N.P.V., T.M.F., A.P.C., V.M.D., and D.L.A.. Photophysical measurements were supported by the National Science Foundation under Grant No. DMR-1752782 supporting J.C. and K.H.. Cytotoxicity measurements were completed by Q.Q. and S.M.S. Mass spectrometric analyses were performed at the University of Tennessee, Knoxville Biological and Small Molecule Mass Spectrometry Core with the assistance of Dr. Shawn R. Campagna, Dr. Hector F. Castro, and Vernon Stafford

### References

1. Paprocka, R.; Wiese-Szadkowska, M.; Janciauskiene, S.; Kosmalksi, T.; Kulik, M.; Helmin-Basa, A., Latest developments in metal complexes as anticancer agents. *Coord. Chem. Rev.* **2022**, *452*, 214307.
2. Gourdon, L.; Cariou, K.; Gasser, G., Phototherapeutic anticancer strategies with first-row transition metal complexes: a critical review. *Chem. Soc. Rev.* **2022**, *51* (3), 1167-1195.
3. Siegel, R. L.; Miller, K. D.; Jemal, A., Cancer statistics, 2020. *CA: A Cancer Journal for Clinicians* **2020**, *70* (1), 7-30.
4. Society, A. C. Global Cancer Facts & Figures. (accessed 9/23/2021).
5. Galanski, M.; Jakupec, M. A.; Keppler, B. K., Update of the preclinical situation of anticancer platinum complexes: novel design strategies and innovative analytical approaches. *Current medicinal chemistry* **2005**, *12* (18), 2075-2094.
6. Johnstone, T. C.; Park, G. Y.; Lippard, S. J., Understanding and Improving Platinum Anticancer Drugs – Phenanthriplatin. *Anticancer research* **2014**, *34* (1), 471-476.
7. Mistry, P.; Kelland, L. R.; Abel, G.; Sidhar, S.; Harrap, K. R., The relationships between glutathione, glutathione-S-transferase and cytotoxicity of platinum drugs and melphalan in eight human ovarian carcinoma cell lines. *British Journal of Cancer* **1991**, *64* (2), 215.



8. Kelland, L., The resurgence of platinum-based cancer chemotherapy. *Nature Reviews Cancer* **2007**, *7* (8), 573.
9. Yang, P.; Ebbert, J. O.; Sun, Z.; Weinshilboum, R. M., Role of the glutathione metabolic pathway in lung cancer treatment and prognosis: a review. *Journal of clinical oncology* **2006**, *24* (11), 1761-1769.
10. Shi, J.; Kantoff, P. W.; Wooster, R.; Farokhzad, O. C., Cancer nanomedicine: progress, challenges and opportunities. *Nature Reviews Cancer* **2017**, *17* (1), 20.
11. Monro, S.; Colón, K. L.; Yin, H.; Roque, J.; Konda, P.; Gujar, S.; Thummel, R. P.; Lilge, L.; Cameron, C. G.; McFarland, S. A., Transition Metal Complexes and Photodynamic Therapy from a Tumor-Centered Approach: Challenges, Opportunities, and Highlights from the Development of TLD1433. *Chemical Reviews* **2019**, *119* (2), 797-828.
12. Imberti, C.; Zhang, P.; Huang, H.; Sadler, P. J., New Designs for Phototherapeutic Transition Metal Complexes. *Angew Chem Int Ed Engl* **2020**, *59* (1), 61-73.
13. Heinemann, F.; Karges, J.; Gasser, G., Critical Overview of the Use of Ru(II) Polypyridyl Complexes as Photosensitizers in One-Photon and Two-Photon Photodynamic Therapy. *Accounts of Chemical Research* **2017**, *50* (11), 2727-2736.
14. Zhang, Y.; Zhou, Q.; Tian, N.; Li, C.; Wang, X., Ru(II)-Complex-Based DNA Photocleaver Having Intense Absorption in the Phototherapeutic Window. *Inorganic Chemistry* **2017**, *56* (4), 1865-1873.
15. Jarvi, M. T.; Patterson, M. S.; Wilson, B. C., Insights into photodynamic therapy dosimetry: simultaneous singlet oxygen luminescence and photosensitizer photobleaching measurements. *Biophys J* **2012**, *102* (3), 661-671.
16. Clement, S.; Deng, W.; Camilleri, E.; Wilson, B. C.; Goldys, E. M., X-ray induced singlet oxygen generation by nanoparticle-photosensitizer conjugates for photodynamic therapy: determination of singlet oxygen quantum yield. *Scientific Reports* **2016**, *6* (1), 19954.
17. Weersink, R. A.; Bogaards, A.; Gertner, M.; Davidson, S. R. H.; Zhang, K.; Natchev, G.; Trachtenberg, J.; Wilson, B. C., Techniques for delivery and monitoring of TOOKAD (WST09)-mediated photodynamic therapy of the prostate: Clinical experience and practicalities. *Journal of Photochemistry and Photobiology B: Biology* **2005**, *79* (3), 211-222.
18. Kohler, L.; Nease, L.; Vo, P.; Garofolo, J.; Heidary, D. K.; Thummel, R. P.; Glazer, E. C., Photochemical and Photobiological Activity of Ru(II) Homoleptic and Heteroleptic Complexes Containing Methylated Bipyridyl-type Ligands. *Inorganic Chemistry* **2017**, *56* (20), 12214-12223.
19. Griffith, C.; Dayoub, A. S.; Jaranatne, T.; Alatrash, N.; Mohamedi, A.; Abayan, K.; Breitbach, Z. S.; Armstrong, D. W.; MacDonnell, F. M., Cellular and cell-free studies of catalytic DNA cleavage by ruthenium polypyridyl complexes containing redox-active intercalating ligands. *Chemical Science* **2017**, *8* (5), 3726-3740.
20. Yadav, A.; Janaratne, T.; Krishnan, A.; Singhal, S. S.; Yadav, S.; Dayoub, A. S.; Hawkins, D. L.; Awasthi, S.; MacDonnell, F. M., Regression of lung cancer by hypoxia-sensitizing ruthenium polypyridyl complexes. *Mol Cancer Ther* **2013**, *12* (5), 643-53.
21. Steinke, S. J.; Gupta, S.; Piechota, E. J.; Moore, C. E.; Kodanko, J. J.; Turro, C., Photocytotoxicity and photoinduced phosphine ligand exchange in a Ru(ii) polypyridyl complex. *Chemical Science* **2022**, *13* (7), 1933-1945.
22. König, K., Multiphoton microscopy in life sciences. *J Microsc* **2000**, *200* (Pt 2), 83-104.

23. Howerton, B. S.; Heidary, D. K.; Glazer, E. C., Strained Ruthenium Complexes Are Potent Light-Activated Anticancer Agents. *Journal of the American Chemical Society* **2012**, *134* (20), 8324-8327.
24. Arora, K.; Herroon, M.; Al-Afyouni, M. H.; Toupin, N. P.; Rohrabough, T. N.; Loftus, L. M.; Podgorski, I.; Turro, C.; Kodanko, J. J., Catch and Release Photosensitizers: Combining Dual-Action Ruthenium Complexes with Protease Inactivation for Targeting Invasive Cancers. *Journal of the American Chemical Society* **2018**, *140* (43), 14367-14380.
25. Al-Afyouni, M. H.; Rohrabough, T. N.; Al-Afyouni, K. F.; Turro, C., New Ru(II) photocages operative with near-IR light: new platform for drug delivery in the PDT window. *Chemical Science* **2018**, *9* (32), 6711-6720.
26. Havrylyuk, D.; Heidary, D. K.; Sun, Y.; Parkin, S.; Glazer, E. C., Photochemical and Photobiological Properties of Pyridyl-pyrazol(in)e-Based Ruthenium(II) Complexes with Sub-micromolar Cytotoxicity for Phototherapy. *ACS Omega* **2020**, *5* (30), 18894-18906.
27. Shi, H.; Imberti, C.; Sadler, P. J., Diazido platinum(IV) complexes for photoactivated anticancer chemotherapy. *Inorganic Chemistry Frontiers* **2019**, *6* (7), 1623-1638.
28. van Rixel, V. H. S.; Ramu, V.; Auyeung, A. B.; Beztsinna, N.; Leger, D. Y.; Lameijer, L. N.; Hilt, S. T.; Le Dévédec, S. E.; Yildiz, T.; Betancourt, T.; Gildner, M. B.; Hudnall, T. W.; Sol, V.; Liagre, B.; Kornienko, A.; Bonnet, S., Photo-Uncaging of a Microtubule-Targeted Rigidin Analogue in Hypoxic Cancer Cells and in a Xenograft Mouse Model. *Journal of the American Chemical Society* **2019**, *141* (46), 18444-18454.
29. Hachey, A. C.; Havrylyuk, D.; Glazer, E. C., Biological activities of polypyridyl-type ligands: implications for bioinorganic chemistry and light-activated metal complexes. *Curr Opin Chem Biol* **2021**, *61*, 191-202.
30. Ashford, D. L.; Glasson, C. R. K.; Norris, M. R.; Hanson, K.; Concepcion, J. J.; Keinan, S.; Brennaman, M. K.; Templeton, J. L.; Meyer, T. J., Controlling Ground and Excited State Properties through Ligand Changes in Ruthenium Polypyridyl Complexes. *Inorg Chem* **2014**, *53* (11), 5637-5646.
31. Reichardt, C.; Monroe, S.; Sobotta, F. H.; Colón, K. L.; Sainuddin, T.; Stephenson, M.; Sampson, E.; Roque, J.; Yin, H.; Brendel, J. C.; Cameron, C. G.; McFarland, S.; Dietzek, B., Predictive Strength of Photophysical Measurements for in Vitro Photobiological Activity in a Series of Ru(II) Polypyridyl Complexes Derived from  $\pi$ -Extended Ligands. *Inorganic Chemistry* **2019**, *58* (5), 3156-3166.
32. Fong, J.; Kasimova, K.; Arenas, Y.; Kaspler, P.; Lazic, S.; Mandel, A.; Lilge, L., A novel class of ruthenium-based photosensitizers effectively kills in vitro cancer cells and in vivo tumors. *Photochem Photobiol Sci* **2015**, *14* (11), 2014-23.
33. Monroe, S.; Colon, K. L.; Yin, H.; Roque, J., 3rd; Konda, P.; Gujar, S.; Thummel, R. P.; Lilge, L.; Cameron, C. G.; McFarland, S. A., Transition Metal Complexes and Photodynamic Therapy from a Tumor-Centered Approach: Challenges, Opportunities, and Highlights from the Development of TLD1433. *Chem Rev* **2019**, *119* (2), 797-828.
34. Thompson, D. W.; Ito, A.; Meyer, T. J., [Ru(bpy)<sub>3</sub>]<sup>2+</sup> and other remarkable metal-to-ligand charge transfer (MLCT) excited states. *Pure and Applied Chemistry* **2013**, *85* (7), 1257-1305.
35. Demas, J. N.; Adamson, A. W., Tris (2,2'-bipyridine)ruthenium(II) sensitized reactions of some oxalato complexes. *J. Amer. Chem. Soc.* **1973**, *95* (16), 5159-68.

36. Bock, C. R.; Meyer, T. J.; Whitten, D. G., Electron transfer quenching of the luminescent excited state of tris(2,2'-bipyridine)ruthenium(II). Flash photolysis relaxation technique for measuring the rates of very rapid electron transfer reactions. *J. Amer. Chem. Soc.* **1974**, *96* (14), 4710-12.
37. Lameijer, L. N.; Ernst, D.; Hopkins, S. L.; Meijer, M. S.; Askes, S. H. C.; Le Dévédec, S. E.; Bonnet, S., A Red-Light-Activated Ruthenium-Caged NAMPT Inhibitor Remains Phototoxic in Hypoxic Cancer Cells. *Angewandte Chemie (International ed. in English)* **2017**, *56* (38), 11549-11553.
38. Respondek, T.; Garner, R. N.; Herroon, M. K.; Podgorski, I.; Turro, C.; Kodanko, J. J., Light Activation of a Cysteine Protease Inhibitor: Caging of a Peptidomimetic Nitrile with Ru(II)(bpy)<sub>2</sub>. *Journal of the American Chemical Society* **2011**, *133* (43), 17164-17167.
39. Zamora, A.; Denning, C. A.; Heidary, D. K.; Wachter, E.; Nease, L. A.; Ruiz, J.; Glazer, E. C., Ruthenium-containing P450 inhibitors for dual enzyme inhibition and DNA damage. *Dalton Transactions* **2017**, *46* (7), 2165-2173.
40. Karges, J.; Heinemann, F.; Jakubaszek, M.; Maschietto, F.; Subecz, C.; Dotou, M.; Vinck, R.; Blacque, O.; Tharaud, M.; Goud, B.; Viñuelas Zahinos, E.; Spingler, B.; Ciofini, I.; Gasser, G., Rationally Designed Long-Wavelength Absorbing Ru(II) Polypyridyl Complexes as Photosensitizers for Photodynamic Therapy. *Journal of the American Chemical Society* **2020**, *142* (14), 6578-6587.
41. Li, A.; Yadav, R.; White, J. K.; Herroon, M. K.; Callahan, B. P.; Podgorski, I.; Turro, C.; Scott, E. E.; Kodanko, J. J., Illuminating cytochrome P450 binding: Ru(II)-caged inhibitors of CYP17A1. *Chemical Communications* **2017**, *53* (26), 3673-3676.
42. Cole, H. D.; Roque, J. A., 3rd; Lifshits, L. M.; Hodges, R.; Barrett, P. C.; Havrylyuk, D.; Heidary, D.; Ramasamy, E.; Cameron, C. G.; Glazer, E. C.; McFarland, S. A., Fine-Feature Modifications to Strained Ruthenium Complexes Radically Alter Their Hypoxic Anticancer Activity(dagger). *Photochem Photobiol* **2022**, *98* (1), 73-84.
43. Wachter, E.; Zamora, A.; Heidary, D. K.; Ruiz, J.; Glazer, E. C., Geometry matters: inverse cytotoxic relationship for cis/trans-Ru(II) polypyridyl complexes from cis/trans-[PtCl<sub>2</sub>(NH<sub>3</sub>)<sub>2</sub>]. *Chemical Communications* **2016**, *52* (66), 10121-10124.
44. Wachter, E.; Heidary, D. K.; Howerton, B. S.; Parkin, S.; Glazer, E. C., Light-activated ruthenium complexes photobind DNA and are cytotoxic in the photodynamic therapy window. *Chemical Communications* **2012**, *48* (77), 9649-9651.
45. Loftus, L. M.; Al-Afyouni, K. F.; Turro, C. A.-O. h. o. o., New Ru(II) Scaffold for Photoinduced Ligand Release with Red Light in the Photodynamic Therapy (PDT) Window. (1521-3765 (Electronic)).
46. Meijer, M. S.; Natile, M. M.; Bonnet, S., 796 nm Activation of a Photocleavable Ruthenium(II) Complex Conjugated to an Upconverting Nanoparticle through Two Phosphonate Groups. *Inorganic Chemistry* **2020**, *59* (20), 14807-14818.
47. Knoll, J. D.; Albani, B. A.; Turro, C., Excited state investigation of a new Ru(II) complex for dual reactivity with low energy light. *Chem Commun (Camb)* **2015**, *51* (42), 8777-80.
48. Caspar, J. V.; Meyer, T. J., Photochemistry of MLCT excited states. Effect of nonchromophoric ligand variations on photophysical properties in the series cis-Ru(bpy)<sub>2</sub>L<sub>2</sub><sup>2+</sup>. *Inorganic Chemistry* **1983**, *22* (17), 2444-53.

49. Durham, B.; Caspar, J. V.; Nagle, J. K.; Meyer, T. J., Photochemistry of tris(2,2'-bipyridine)ruthenium(2+) ion. *Journal of the American Chemical Society* **1982**, *104* (18), 4803-10.
50. Anderson, P. A.; Strouse, G. F.; Treadway, J. A.; Keene, F. R.; Meyer, T. J., Black MLCT Absorbers. *Inorg. Chem.* **1994**, *33* (18), 3863-4.
51. Anderson, P. A.; Keene, F. R.; Meyer, T. J.; Moss, J. A.; Strouse, G. F.; Treadway, J. A., Manipulating the properties of MLCT excited states. *Journal of the Chemical Society, Dalton Transactions: Inorganic Chemistry (1972-1999)* **2002**, (20), 3820-3831.
52. Caspar, J. V.; Meyer, T. J., Photochemistry of tris(2,2'-bipyridine)ruthenium(2+) ion (Ru(bpy)<sub>3</sub><sup>2+</sup>). Solvent effects. *Journal of the American Chemical Society* **1983**, *105* (17), 5583-5590.
53. Qu, F.; Lamb, R. W.; Cameron, C. G.; Park, S.; Oladipupo, O.; Gray, J. L.; Xu, Y.; Cole, H. D.; Bonizzoni, M.; Kim, Y.; McFarland, S. A.; Webster, C. E.; Papish, E. T., Singlet Oxygen Formation vs Photodissociation for Light-Responsive Protic Ruthenium Anticancer Compounds: The Oxygenated Substituent Determines Which Pathway Dominates. *Inorganic Chemistry* **2021**, *60* (4), 2138-2148.
54. Leblanc, N.; Sproules, S.; Fink, K.; Sanguinet, L.; Alévêque, O.; Levillain, E.; Rosa, P.; Powell, A. K., A fascinating multifaceted redox-active chelating ligand: introducing the N,N'-dimethyl-3,3'-biquinoxalium "methylbiquinoxen" platform. *Chemical Science* **2016**, *7* (6), 3820-3828.
55. Norris, M. R.; Concepcion, J. J.; Glasson, C. R. K.; Fang, Z.; Lapidés, A. M.; Ashford, D. L.; Templeton, J. L.; Meyer, T. J., Synthesis of Phosphonic Acid-Derivatized Bipyridine Ligands and Their Ruthenium Complexes. *Inorganic Chemistry* **2013**, *52* (21), 12492-12501.
56. Gu, J.; Chen, J.; Schmehl, R. H., Using Intramolecular Energy Transfer to Transform non-Photoactive, Visible-Light-Absorbing Chromophores into Sensitizers for Photoredox Reactions. *Journal of the American Chemical Society* **2010**, *132* (21), 7338-7346.
57. Lever, A. B. P., Electrochemical parametrization of metal complex redox potentials, using the ruthenium(III)/ruthenium(II) couple to generate a ligand electrochemical series. *Inorganic Chemistry* **1990**, *29* (6), 1271-85.
58. Yam, V. W.-W.; Lee, V. W.-M.; Ke, F.; Siu, K.-W. M., Synthesis, Photophysics, and Electrochemistry of Ruthenium(II) Polypyridine Complexes with Crown Ether Pendants. *Inorganic Chemistry* **1997**, *36* (10), 2124-2129.
59. Rillema, D. P.; Mack, K. B., The low-lying excited state in ligand  $\pi$ -donor complexes of ruthenium(II): mononuclear and binuclear species. *Inorganic Chemistry* **1982**, *21* (10), 3849-54.
60. Ackermann, M. N.; Interrante, L. V., Ruthenium(II) complexes of modified 1,10-phenanthrolines. 1. Synthesis and properties of complexes containing dipyrindophenazines and a dicyanomethylene-substituted 1,10-phenanthroline. *Inorganic Chemistry* **1984**, *23* (24), 3904-11.
61. Saleh, F. S.; Rahman, M. R.; Okajima, T.; Mao, L.; Ohsaka, T., Determination of formal potential of NADH/NAD<sup>+</sup> redox couple and catalytic oxidation of NADH using poly(phenosafranin)-modified carbon electrodes. *Bioelectrochemistry* **2011**, *80* (2), 121-127.
62. Khazim, K.; Giustarini, D.; Rossi, R.; Verkaik, D.; Cornell, J. E.; Cunningham, S. E. D.; Mohammad, M.; Trochta, K.; Lorenzo, C.; Folli, F.; Bansal, S.; Fanti, P., Glutathione redox

- potential is low and glutathionylated and cysteinylated hemoglobin levels are elevated in maintenance hemodialysis patients. *Transl Res* **2013**, *162* (1), 16-25.
63. Caspar, J. V.; Kober, E. M.; Sullivan, B. P.; Meyer, T. J., Application of the energy gap law to the decay of charge-transfer excited states. *J. Am. Chem. Soc.* **1982**, *104* (2), 630-632.
64. White, J. K.; Schmehl, R. H.; Turro, C., An overview of photosubstitution reactions of Ru(II) imine complexes and their application in photobiology and photodynamic therapy. *Inorganica Chimica Acta* **2017**, *454*, 7-20.
65. Singh, T. N.; Turro, C., Photoinitiated DNA Binding by cis-[Ru(bpy)<sub>2</sub>(NH<sub>3</sub>)<sub>2</sub>]<sup>2+</sup>. *Inorganic Chemistry* **2004**, *43* (23), 7260-7262.
66. Durham, B.; Wilson, S. R.; Hodgson, D. J.; Meyer, T. J., Cis-trans photoisomerization in Ru(bpy)<sub>2</sub>(OH<sub>2</sub>)<sub>2</sub><sup>2+</sup>. Crystal structure of trans-[Ru(bpy)<sub>2</sub>(OH<sub>2</sub>)(OH)](ClO<sub>4</sub>)<sub>2</sub>. *Journal of the American Chemical Society* **1980**, *102* (2), 600-607.
67. Gama Sauaia, M. I.; Tfouni, E.; Helena de Almeida Santos, R.; Teresa do Prado Gambardella, M.; Del Lama, M. P. F. M.; Fernando Guimarães, L.; Santana da Silva, R., Use of HPLC in the identification of cis and trans-diaquabis(2,2'-bipyridine)ruthenium(II) complexes: crystal structure of cis-[Ru(H<sub>2</sub>O)<sub>2</sub>(bpy)<sub>2</sub>](PF<sub>6</sub>)<sub>2</sub>. *Inorganic Chemistry Communications* **2003**, *6* (7), 864-868.
68. Hidayatullah, A. N.; Wachter, E.; Heidary, D. K.; Parkin, S.; Glazer, E. C., Photoactive Ru(II) Complexes With Dioxinophenanthroline Ligands Are Potent Cytotoxic Agents. *Inorganic Chemistry* **2014**, *53* (19), 10030-10032.
69. Wachter, E.; Glazer, E. C., Mechanistic Study on the Photochemical "Light Switch" Behavior of [Ru(bpy)<sub>2</sub>dmdppz]<sup>2+</sup>. *The Journal of Physical Chemistry A* **2014**, *118* (45), 10474-10486.
70. Sun, Q.; Mosquera-Vazquez, S.; Suffren, Y.; Hankache, J.; Amstutz, N.; Lawson Daku, L. M.; Vauthey, E.; Hauser, A., On the role of ligand-field states for the photophysical properties of ruthenium(II) polypyridyl complexes. *Coordination Chemistry Reviews* **2015**, *282-283*, 87-99.
71. Sun, Q.; Mosquera-Vazquez, S.; Lawson Daku, L. M.; Guénee, L.; Goodwin, H. A.; Vauthey, E.; Hauser, A., Experimental Evidence of Ultrafast Quenching of the 3MLCT Luminescence in Ruthenium(II) Tris-bipyridyl Complexes via a 3dd State. *Journal of the American Chemical Society* **2013**, *135* (37), 13660-13663.
72. Li, J.; Djurovich, P. I.; Alleyne, B. D.; Yousufuddin, M.; Ho, N. N.; Thomas, J. C.; Peters, J. C.; Bau, R.; Thompson, M. E., Synthetic Control of Excited-State Properties in Cyclometalated Ir(III) Complexes Using Ancillary Ligands. *Inorg. Chem.* **2005**, *44* (6), 1713-1727.
73. Gorelsky, S. I.; Dodsworth, E. S.; Lever, A. B. P.; Vlcek, A. A., Trends in metal-ligand orbital mixing in generic series of ruthenium N-donor ligand complexes - effect on electronic spectra and redox properties. *Coord. Chem. Rev.* **1998**, *174*, 469-494.
74. Kober, E. M.; Marshall, J. L.; Dressick, W. J.; Sullivan, B. P.; Caspar, J. V.; Meyer, T. J., Synthetic control of excited states. Nonchromophoric ligand variations in polypyridyl complexes of osmium(II). *Inorg. Chem.* **1985**, *24* (18), 2755-63.
75. Jortner, J., Radiationless transitions. *Pure and Applied Chemistry* **1971**, *27* (3), 389-420.
76. Van Houten, J.; Watts, R. J., Temperature dependence of the photophysical and photochemical properties of the tris(2,2'-bipyridyl)ruthenium(II) ion in aqueous solution. *Journal of the American Chemical Society* **1976**, *98* (16), 4853-8.

77. Thompson, D. W.; Fleming, C. N.; Myron, B. D.; Meyer, T. J., Rigid medium stabilization of metal-to-ligand charge transfer excited states. *Journal of Physical Chemistry B* **2007**, *111* (24), 6930-6941.